

**THE EFFECTS OF SECONDARY STATIONARY-PHASE POLYMERS
ON ADSORPTION AND TRANSPORT
IN ION-EXCHANGE CHROMATOGRAPHY**

by

Matthew G. Petroff

A thesis submitted to the Faculty of the University of Delaware in partial fulfillment of the requirements for the degree of Honors Bachelor of Chemical Engineering with Distinction

Spring 2009

Copyright 2009 Matthew G. Petroff
All Rights Reserved

**THE EFFECTS OF SECONDARY STATIONARY-PHASE POLYMERS
ON ADSORPTION AND TRANSPORT
IN ION-EXCHANGE CHROMATOGRAPHY**

by

Matthew G. Petroff

Approved: _____
A.M. Lenhoff, PhD
Professor in charge of thesis on behalf of the Advisory Committee

Approved: _____
C.J. Roberts, PhD
Committee member from the Department of Chemical Engineering

Approved: _____
M. Keefe, PhD
Committee member from the Board of Senior Thesis Readers

Approved: _____
Alan Fox, Ph.D.
Director, University Honors Program

TABLE OF CONTENTS

LIST OF TABLES	v
LIST OF FIGURES	vi
ABSTRACT	viii
Chapter	
1 INTRODUCTION	1
1.1 Background and Motivation	1
1.2 Chromatography	5
1.3 Goals and Thesis Outline.....	8
2 THEORY	10
2.1 Adsorption	10
2.2 Transport.....	14
2.3 Linear Isocratic Retention.....	19
3 MATERIALS AND METHODS	20
3.1 Materials	20
3.1.1 Adsorbents.....	20
3.1.2 Columns.....	22
3.1.3 Proteins.....	23
3.1.4 Buffer Solutions	25
3.2 Methods	26
3.2.1 Isotherm Determination.....	26
3.2.1 Batch Uptake	27
3.2.2 Isocratic Retention.....	30
4 RESULTS AND DISCUSSION	32

4.1 Isocratic Pulse Response	32
4.1 Adsorption Isotherms	37
4.2 Batch uptake	45
5 CONCLUSIONS AND IMPLICATIONS.....	52
REFERENCES	56

LIST OF TABLES

Table 3.1: Resin properties for the two resins studied, as reported by the manufacturer	21
Table 3.2: Measured void fraction for adsorbents, after settling under gravity.....	22
Table 3.3: Relevant physiochemical properties of the two proteins used in this study.....	25
Table 3.4: Phase ratios used in the fits of isotherm data to the colloidal isotherm model.	27
Table 4.1: Parameters obtained from a fit of k' data to $\ln(k') = m * \ln (IS) + b$	34

LIST OF FIGURES

Figure 3.1: Example run from a separation of lactoferrin using Sepharose FF.....	24
Figure 3.2: Schematic of experimental apparatus used in batch uptake experiments.	28
Figure 3.3: Calibration of the Akta UV flow cell for different lysozyme concentrations.....	29
Figure 4.1: k' data for lysozyme on SP-650 M (red), lysozyme on GigaCap (blue), and lactoferrin on SP 650-M (black).	34
Figure 4.2: Elution profiles from isocratic pulse reponse experiments of lactoferrin on GigaCap.	37
Figure 4.3: Adsorption isotherms for lysozyme on GigaCap at 2 mM (black), 6 mM (red), 20 mM (blue), 50 mM (green) and 100 mM (gray) ionic strengths.....	39
Figure 4.4: Adsorption isotherms for lactoferrin onto GigaCap at 20 mM (black), 50 mM (red) and 200 mM (blue) ionic strength.	41
Figure 4.5: Adsorption isotherms for lactoferrin onto SP 650 M at 20 (black), 50 mM (red), and 200 mM (blue) ionic strength, pH 7.....	42
Figure 4.6: Variation of static capacities with ionic strength for lysozyme on GigaCap and SP 650M.	44
Figure 4.7: Variation of static capacities with ionic strength for lactoferrin onto GigaCap and SP 650M.	45
Figure 4.8: Lactoferrin uptake on GigaCap for solution pH 7.0 and ionic strengths of 20 mM (black), 50 mM (blue), and 200 mM.....	47
Figure 4.9: Lysozyme uptake on GigaCap for solution pH 7.0 and ionic strengths of 6 mM (black), 20 mM (blue), and 100 mM (red). Solid lines are fits to the shrinking core model.	48

Figure 4.10: Lysozyme uptake onto SP-650 for solution pH 7.0 and ionic strengths of 6 mM (black), 20 mM (blue), and 100 mM (red)..... 49

Figure 4.11: Lactoferrin uptake onto SP-650M for solution pH 7.0 and ionic strengths of 20 mM (black), 50 mM (blue), and 200 mM..... 50

Figure 4.12: The effect of ionic strength on the normalized effective diffusivity (D_e/D_0) of lysozyme and lactoferrin on GigaCap and SP 650M. 51

ABSTRACT

Recent attempts to improve the adsorption and transport properties of ion-exchange adsorbents have included the modification of the adsorbent base matrix with a secondary polymer layer. This work attempts to characterize the relevant adsorption and transport properties of two related strong cation exchange adsorbents, Toyopearl GigaCap and Toyopearl SP-650M, which differ in that the GigaCap adsorbent consists of the SP-650M base matrix functionalized with a secondary-polymer layer. The studies performed utilized a combination of equilibrium adsorption isotherm determination, batch uptake, and isocratic pulse response experiments. Results were obtained for two model proteins, lysozyme (14.7 kDa) and lactoferrin (78 kDa), and were compared between the adsorbents to allow for elucidation of the effects of protein charge, protein size, and GigaCap's secondary-polymer layer on the transport and adsorption behavior.

The batch uptake results indicate higher effective pore diffusivities for lysozyme than for lactoferrin, but similar effective pore diffusivities for the respective proteins in the two adsorbents. The adsorption isotherms indicate that both proteins display much higher static capacities for the GigaCap S-650M particles than for the SP 650M particles. While the capacity differences are significant at low ionic strengths, they are drastically reduced at high ionic strengths, a trend that is more significant in

lactoferrin than lysozyme. Retention experiments indicate decreasing retention between the protein-adsorbent pairs of lactoferrin on SP-650M, lysozyme on GigaCap, and lysozyme on SP-650M, as well as evidence of lactoferrin exclusion from GigaCap's secondary polymer layer. Taken together, the adsorption and retention experiments indicate that lactoferrin is excluded from GigaCap's secondary polymer layer high ionic strengths, and is partially excluded at lower ionic strengths. This exclusion appears to be a combination of steric effects, due to conformational changes in the polymer layer that reduce the accessibility for protein binding due to polymer shrinkage at high ionic strengths, and a decrease in the electrostatic forces that drive solute partitioning into the polymer layer. These effects are most significant at high ionic strengths, where lactoferrin is excluded from the polymer layer, but also appear at lower ionic strengths, where large differences in lactoferrin capacity are observed between ionic strengths of 20 mM and 50 mM.

This exclusion behavior is observed for ionic strengths that are relevant for chromatographic process operations. It is thus important to be aware of these effects during process design, as relatively small ionic strength deviations may result in drastic changes in process performance. It is also relevant to future resin design, as it may be desirable to either reduce or exploit these effects in future adsorbents. Specifically, it presents an opportunity to design ion-exchange resins that have high affinity for ions of a specific molecular size range. It also demonstrates that changes

must be made to the nature of the polymer layer before these adsorbents can display robust, high capacities for larger macromolecules.

Chapter 1

INTRODUCTION

1.1 Background and Motivation

The advent of the molecular biology revolution has drastically changed the pharmaceutical industry¹. Specifically, recent advances in the fields of genomics and information technology have converged to impart improved capabilities for drug discovery and production to pharmaceutical companies. These advances include both fundamental achievements, such as the sequencing of the human genome² and the establishment of the Protein Data Bank (PDB)³, and improvements in the underlying molecular biology techniques behind drug research and production. Such advances have not only led to methods for rational drug design, but have increased the number of biological targets available for treatment.

These technological advances have been most influential in the biotechnological production of biopharmaceutical agents, i.e., the production of product molecules, such as drug agents, by growth in cell culture¹. Biopharmaceutical drug agents may range from viral and DNA vaccines to therapeutic proteins, including

monoclonal antibodies (mAb), which represent the largest class of biologics on the market and in development pipelines.

Biopharmaceutical drug production has experienced rapid growth throughout the last decade. The global market for biopharmaceutical therapeutics was US\$48 billion in 2004, and has been projected to rise beyond US\$100 billion in 2010⁴. The year 2008 also saw 28 new biotechnological IPOs, with financing and partnership deals raising almost US\$45 billion for US companies alone⁵. This expansion has not been exclusive to smaller biotechnology firms; several of the major pharmaceutical companies have included the expansion of biotechnological capabilities in partnerships, deals, and corporate initiatives⁶.

These market forces exert significant pressure for the economical and efficient manufacture of biopharmaceutical products. Biotechnology processes typically consist of an upstream process, where the target molecules are produced in cell culture, and a downstream process, which isolates and packages the target molecules⁷. Recent advances in cell culture, which have led to increased product titers, have caused downstream purification to be the most significant process contribution towards production costs⁸.

A typical downstream biopharmaceutical process can be separated into three distinct stages, each with a different purpose: capture, separation and polishing⁹. Capture involves the removal of target drugs from their host cells. Cells are lysed, and a combination of centrifugation and filtration is used to remove host cell debris.

Affinity chromatography is often used to isolate the target molecules of interest from the remaining solution⁹. Separation then removes many of the remaining contaminants, such as DNA, host cell proteins and viruses¹⁰. These steps typically utilize multiple chromatography steps in series, such as ion exchange or hydrophobic interaction chromatography. Polishing then removes the remaining closely related impurities, stabilizes, and packages the drug agent¹¹. Polishing may also consist of several unit operations, including chromatography, ultrafiltration, diafiltration, and crystallization⁷.

Chromatography is widely used throughout downstream processes because it offers a large number of advantages that are specially suited for pharmaceutical applications. These advantages include high selectivity, robustness, bio-compatible operating conditions, low-cost operating conditions, and batch operation, all of which are needed to meet the stringent demands set by the FDA¹². Of the various chromatographic methods available, ion-exchange (IEX) is especially useful because adsorption characteristics—and thus purification ability-- depend on many factors, including pH, solution ionic strength and adsorbent chemistry¹³. Small changes in any of these parameters can drastically change elution profiles, thus making IEX one of the most flexible purification methods available.

The main drawback of chromatography is that process design is complex and relies heavily on empirical data¹³. Many of the relevant thermodynamic and transport theories have been developed for application to solutions of small molecules, but are

not entirely appropriate for use in chromatographic process modeling. A priori design is also complicated by both the poorly characterized nature, and the complexity, of chromatographic adsorbents and fermentation broths¹³. While many attempts have been made to predict chromatographic elution profiles^{14,15}, such predictions typically correspond to unrealistically simple solution and operating conditions, and rely on an extremely large body of experimental data. Although promising, these predictions are too limited for immediate application in process design, and reflect a fundamental gap in the knowledge and understanding of chromatographic adsorption and transport mechanisms. A greater understanding of these mechanisms is necessary for improved process design, and may even aid in improved adsorbent design¹⁶.

Efforts to better understand the chromatographic performance characteristics of different adsorbent materials have adopted two main strategies. The first strategy has focused on the characterization of adsorbent structure and its effects on adsorption, transport, and elution^{16,17,18,19}. This strategy has focused primarily on the experimental determination of the relevant chromatographic parameters for different adsorbent materials. Such experiments include bulk measurements of overall adsorbent properties on a column scale, and are often coupled with microscopic methods, which measure the properties of an individual adsorbent particle¹⁸. These experimentally determined parameters can be compared across different adsorbent materials, and are often applied in the modeling of chromatographic process behavior¹¹. The second strategy has focused on the development of theories that are both more suitable and

more practical descriptions of macromolecular adsorption. These have included descriptions of bulk adsorption^{20,21} and transport behavior²², as well as microscopic models of adsorbent profiles during solute uptake^{23,24}.

1.2 Chromatography

In liquid chromatography, a liquid solution containing several different solute molecules, termed the mobile phase, is passed through a column packed with a solid adsorbent, termed the stationary phase. The molecules in the mobile phase can partition between the liquid and a physically adsorbed state on the stationary phase, which retards the solute's migration velocity through the column. Separation arises from the differences in migration velocities between solutes, as low-affinity solutes elute first and high-affinity solutes elute last¹².

The adsorbent-solute interactions are governed by a combination of physical forces, the most significant of which are van der Waals, electrostatic and hydrophobic forces¹³. The strengths of these interactions are governed by a combination of adsorbent chemistry, solute chemistry and solution conditions²⁵. Differences in adsorption partitioning, and thus the chromatographic selectivity, between two solutes can then be obtained by manipulation of adsorbent structure, adsorbent chemistry, or mobile phase composition.

Stationary phases are usually functionalized with specialized ligand chemistries to take advantage of the different solute-adsorbent physical interactions. Examples of

ligand chemistry types that are used in biotechnological processes include metal ion, hydrophobic interaction, and ion-exchange¹². Of these, ion-exchange adsorbents are the most commonly used, and are found in over 40% of biotechnological chromatography process steps²⁶. Adsorption in ion-exchange is primarily governed by electrostatic interactions between the solute and adsorbent²⁷. Ion-exchange adsorbents can be divided into four general classes, as determined by the nature of the functional ligand. Strong cation-exchangers are usually functionalized with sulfopropyl ligands (SP), weak cation exchangers with carboxymethyl ligands (CM), strong anion exchangers with quaternary amines (Q) and weak anion exchangers with diethyl amines (DEAE)²⁷.

The adsorbent structure is primarily dictated by the base matrix, examples of which are cellulose, dextran, agarose and polyacrylamide. Silica is widely used in analytical separations, but less so for preparative applications in biotechnology due to issues with chemical stability during cleaning¹². Polymeric adsorbent beads are formed by cross-linking the base polymer. Adsorbent geometry can be controlled by variation of both the cross-linker density and the synthesis strategy. A high cross-linker density results in adsorbent matrices with small pore sizes and high surface area to volume ratios. A high crosslinker density also increases mechanical strength, allowing for increased process flow rates.

One method of changing adsorption behavior by modifying adsorbent geometry is the attachment of secondary polymers onto a traditional base matrix. The first such

resins with such polymer-modified backbones consisted of linear branched polymers that were end-grafted onto the adsorbent base matrix²⁸. These tentacle-type secondary polymers are fused with functional ligands, which increases the accessibility of the ligands to adsorbate when compared to traditional adsorbents. Studies have shown that these adsorbents possess a high degree of variation in accessible surface area with changes in ionic strength, due to the flexible nature of the tentacles²⁹. Another polymer-modification approach has involved filling the pore volume of an adsorbent shell with a functionalized gel, such as polyacrylamide²⁴ or agarose²⁵. These adsorbents also exhibit much higher static capacities than traditional resins, but display much less variation in accessible surface area with ionic strength.

A final polymer-modification method has involved grafting branched polymers, such as dextrans, which may also be functionalized with ion-exchange ligands, to the adsorbent base matrix. These adsorbents possess less variation in accessible surface area with ionic strength than the tentacle-type exchangers, but occupy a smaller fraction of the pore space than the “gel in a shell” exchangers²⁸. Examples of this class of adsorbent include GE Healthcare’s Sepharose XL, and Tosoh Bioscience’s GigaCap adsorbent lines. Although the effects of these polymers on chromatographic performance are incompletely understood, some studies suggest that they convey favorable transport and adsorption properties^{25,28}. While the design and use of these adsorbents may be desirable, the current lack of knowledge regarding their behavior limits their effectiveness.

1.3 Goals and Thesis Outline

This research focuses on the recent efforts, noted above, to alter the adsorption characteristics of adsorbent materials by attaching secondary polymers to a more traditional adsorbent matrix. The goal of this work is to better understand the effects of these secondary polymers on the adsorption and transport properties of their base materials, such as protein capacities and intraparticle transport rates. This increased knowledge is applicable to the design of future resins, and may also aid in the design of future chromatographic processes.

Two adsorbents were selected for this investigation, Tosoh Bioscience's Toyopearl SP-650M and Toyopearl GigaCap S-650M. Both materials are strong cation exchangers, and consist of sulfopropyl ligands functionalized on the same base matrix. These adsorbents differ mainly in that GigaCap contains secondary polymers, which allows for a direct comparison between the adsorption and transport properties of the two materials that can provide insight into the mechanisms governing the behavior and performance imparted by the secondary polymers. Experiments utilized the two model proteins, lysozyme (MW=14.7 kDa) and lactoferrin (MW=78 kDa), in order to make a comparison for the effects of protein size on resin behavior. Resin properties were determined using a combination of isotherm determination, isocratic retention measurements and batch uptake.

Chapter 2 outlines the basic chromatographic theory relevant to this thesis. Chapter 3 then provides a detailed description of the experimental materials and methods used for the work. Chapter 4 displays and describes the findings concerning both the characterization of the two cation exchangers, as well as a comparison between their adsorption and transport properties.

Chapter 2

THEORY

2.1 Adsorption

Chromatographic separation occurs due to the differences in the partitioning of solutes between the stationary phase and the mobile phase. These are fundamentally equilibrium effects, and are mechanistically described by the static adsorption of a solute onto the surface of a chromatographic stationary phase. Adsorption is dictated by a combination of accessible surface area (geometry and pore size distribution)³⁰, solute-solute interactions, and solute-adsorbent interactions, which are primarily electrostatic in IEX²⁰. These equilibrium effects are usually characterized using adsorption isotherms, which are commonly determined by measuring the equilibrium uptake of a solute onto an adsorbent.

Plots of adsorption isotherms can be divided into two main regions, a linear region and a plateau. The linear region is seen at low bulk solution concentrations, and is where the adsorbed concentration is directly proportional to the bulk solution concentration³¹. It corresponds to a situation of low fractional loading, where solute-solute interactions are negligible²⁰. The slope of the linear region is related to the

strength of the adsorbent-solute interactions; it approaches infinity for strong interactions, and approaches zero for no interactions²⁰. Isotherms with very steep linear regions are favorable for adsorption, and isotherms with shallow linear regions are favorable for desorption. The plateau occurs at high bulk concentrations of solute, where adsorption has approached saturation. Adsorption in this region is thus roughly invariant with bulk concentration, and an adsorbent's static capacity can be defined by the concentration of adsorbed solute in this region. In practice, it is usually found that an adsorbent's static capacity for a macromolecule is below its total ion-exchange capacity. This limitation is thought to be due to a combination of solute-adsorbent and solute-solute steric factors, attenuation of solute-adsorbent electrostatic attraction, and solute-solute electrostatic repulsion^{21,31}.

Two limiting cases of isotherm behavior are linear and rectangular isotherms²⁷. Linear isotherms typically occur when only the linear region of the isotherm is represented, and represent a scenario with negligible adsorbate-adsorbate interactions^{20,31}. The assumption of linear isotherm behavior is thus only applicable under low bulk concentrations, and low fractional loading of the adsorbent. Conversely, rectangular isotherms represent the case when the slope of the linear region is infinite, there is no transition region between the linear region and plateau, and the plateau is constant²⁷. Rectangular isotherm behavior represents situations with extremely attractive adsorbent-solute interactions, and negligible solute-solute interactions.

Adsorption isotherms are usually characterized by fits to appropriate isotherm models. Of the potential models for protein adsorption, the Langmuir isotherm is a simple and convenient one for describing the full nonlinear form of the isotherm²⁷.

This model is given by

$$q = \frac{q_s KC}{1 + KC} \quad 2.1$$

where q is the adsorbed quantity, C is the bulk concentration, q_s is the maximum adsorbed concentration, and K is the adsorbate's equilibrium constant between the adsorbed phase and the free solution. This model is based on a mass action model of adsorbate interactions with fixed adsorption sites. It is not mechanistically applicable to macromolecules adsorption, due to the assumptions of fixed adsorption sites and negligible adsorbate-adsorbate interactions. For protein chromatography, therefore, it may be considered semi-empirical, and it does not provide insight into adsorption mechanisms or energetics³².

A more mechanistic alternative isotherm model is based on the use of a colloidal model, which can be expressed as

$$\begin{aligned}
C &= \frac{\Phi}{K_{eq}} q \exp \left[B_{pp} \left(\sqrt{q^*} + \beta \right) \exp \left(\frac{\omega}{\sqrt{q^*}} \right) \right] \\
\alpha &= \frac{9}{2} \exp \left(\frac{\kappa a}{\sqrt{3} N_A} \right) \sqrt{\frac{\sqrt{3} N_A}{2 \phi MW}} \\
\beta &= \frac{3}{2} \exp \left(\frac{\kappa a}{\sqrt{3} N_A} \right) \\
\omega &= - \frac{2 \kappa}{\sqrt{\frac{\sqrt{3} N_A}{2 \phi MW}}}
\end{aligned}
\tag{2.2}$$

where q and C are the same as before. This model attempts to characterize adsorption using four main parameters: K_{eq} is the surface equilibrium constant, representing protein-adsorbent interactions; B_{pp} is the Yukawa constant, and characterizes protein-protein interactions; κ is the Debye parameter, is determined by the salt composition and concentration, and characterizes the length-scales of electrostatic interactions; and ϕ , the phase ratio, is the adsorbent's accessible surface area to volume ratio.

Additional parameters are material constants, and depend on the nature of the system: N_A is Avogadro's number, MW is molecular weight, and a is the protein radius. This equation is based on approximating the adsorbent surface as flat, and the solute molecules as spherical ions with pairwise additive interactions. The colloidal isotherm equation has been shown to be valid for traditional adsorbents, where adsorption typically occurs in a monolayer³³. However, evidence suggests that adsorption onto polymer-modified adsorbents may be interpreted more as volumetric partitioning³⁰. The colloidal model may thus be unsuitable for mechanistic description of adsorption

onto the polymer-modified materials due to its assumption of monolayer surface adsorption²⁸. However, like the Langmuir model, it may be useful for empirical description of adsorption data.

2.2 Transport

Preparative chromatography of macromolecules is subject to mass-transfer limitations that become significant given the operating velocities of preparative process applications²². These limitations are especially important to account for in IEX, because of the strong and long-range nature of the adsorbent-solute ionic interactions. Intraparticle transport, in particular, is generally considered to be the main limitation on process efficiency in an IEX operation²⁷.

Many quantitative models have been developed to describe intraparticle transport in chromatography, the most commonly used of which are the pore diffusion, and homogeneous diffusion models^{34,35}. The pore diffusion model assumes that solute transport on the adsorbent surface is negligible. Transport occurs only through the adsorbent pores, and is accompanied by parallel adsorption onto the adsorbent surface. In ion-exchange, pore diffusion is typically observed under conditions with strong solute-adsorbent attractions, i.e. low ionic strengths and highly charged proteins, as well as adsorbents with large pore size distributions. Under an isotherm that is favorable for adsorption, the pore diffusion model typically generates concentration

profiles with sharp transitions between the saturated and unsaturated regions of an adsorbent¹¹.

In contrast, the surface diffusion model assumes that adsorbed molecules freely diffuse according to a surface concentration flux²⁷. This model is based on Fickian diffusion in a spherical particle, and results in diffuse concentration profiles.

Homogeneous diffusion is typically observed under solution conditions with weak solute-adsorbent interactions, i.e. high ionic strengths and proteins with a low net charge²².

The uptake of a solute into an adsorbent particle can be modeled as diffusion through a spherical particle, with an external source from which the adsorbate is transferred to the particle surface. The general rate model describing transport through a chromatographic adsorbent particle accounts for both pore diffusion and surface or solid diffusion, and is described, with the appropriate boundary and initial conditions, by²⁷

$$\frac{\partial q}{\partial t} = \frac{1}{r^2} \frac{\partial}{\partial r} \left[r^2 \left(\varepsilon_p D_p \frac{\partial c}{\partial r} + D_s \frac{\partial q}{\partial r} \right) \right] \quad 2.3$$

$$t = 0 : c = 0; q = 0$$

$$r = 0 : \frac{\partial c}{\partial r} = 0$$

$$r = r_p : \varepsilon_p D_p \frac{\partial c}{\partial r} + D_s \frac{\partial q}{\partial r} = k_f (C - c)$$

where the independent variables are time, t ; axial position, z ; and intraparticle radial position, r . In addition, C is the concentration in the stationary phase pore lumen; k_f is the external mass transfer coefficient associated with particle loading; ε_p is the particle porosity; D_p is the pore diffusivity; D_e is the surface diffusivity; and r_p is the particle radius.

Assuming local equilibrium between the pore and stationary phase, an effective pore diffusivity can then be written as²⁷

$$D_e = \varepsilon_p D_p + D_s \frac{dq}{dC} \quad 2.4$$

Here the factor dq/dC is the slope of the adsorption isotherm, which implies that D_e is only invariant with bulk concentration for the cases of linear or rectangular isotherms. The intraparticle transport model thus reduces to a homogeneous diffusion model when $\varepsilon_p D_p$ approaches zero, and a pore diffusion model when $D_s dq/dC$ approaches zero.

One limit of the pore diffusion model exists for the case of a rectangular isotherm, which was described in the previous section. This scenario results in shrinking-core behavior, and is characterized by a “shock” front, where the radial concentration profile displays a sharp transition from full saturation to zero,^{18,24} and the radial location of the shock front moves inward as more solute is adsorbed. This shrinking-core behavior represents a transport scenario where the isotherm is perfectly rectangular, and uptake is limited by intraparticle diffusion, i.e., the external mass

transfer resistance associated with adsorbent loading is negligible. Shrinking core behavior can be modeled by¹¹

$$\frac{\varepsilon_p D_p c_b}{R^2 q_s} = \left(\left(1 - \frac{1}{Bi} \right) \eta^2 - \eta \right) \frac{d\eta}{dt} \quad 2.5$$

where $\eta = R_f/R$ is the normalized front position and Bi , the Biot number, is defined as

$$Bi = k_f R / (\varepsilon_p D_p).$$

For a case with varying bulk concentration, such as a batch system, uptake behavior can be analyzed using¹¹

$$\frac{\varepsilon_p D_p c_b}{R^2 q_s} t = \left(1 - \frac{1}{Bi} \right) I_2 - I_1 \quad 2.6$$

where I_1 and I_2 are the shrinking core terms, and are defined as:

$$I_1 = \frac{1}{6\Lambda\lambda} \ln \left[\frac{(1-\Lambda-\Lambda\eta^3)(\lambda+1)}{(\eta+\lambda)^3} \right] + \frac{1}{\Lambda\lambda\sqrt{3}} \left[\tan^{-1} \left(\frac{2\eta-\lambda}{\lambda\sqrt{3}} \right) - \tan^{-1} \left(\frac{2-\lambda}{\lambda\sqrt{3}} \right) \right] \quad 2.7$$

$$I_2 = \frac{1}{3\Lambda} \ln \left[\frac{\lambda^3 + \eta^3}{\lambda^3 + 1} \right] \quad 2.8$$

where λ is defined as

$$\lambda = \left(\frac{1}{\check{c}} - 1 \right)^{\frac{1}{3}} \quad 2.9$$

and Λ is the fractional amount of solute initially present that is taken up by the adsorbent at the end of uptake, and can be obtained from a mass balance

($\Lambda = q_s V_{ads} / (c_0 V)$). The mass transfer coefficient associated with loading into an adsorbent particle is incorporated in Bi , and can be estimated from empirical correlations for the Sherwood number, Sh ¹⁸.

Although the shrinking core model is most applicable under the conditions of a rectangular isotherm, it has been found to be useful in fitting uptake data when the isotherm is farther from the rectangular limit as well²². Such fits typically utilize non-linear regression methods, and can provide estimates for the effective pore diffusivity. The effective pore diffusivities can be compared across adsorbents, proteins, and experimental conditions, and provide insight into transport mechanisms.

2.3 Linear Isocratic Retention

Isocratic retention under linear chromatography conditions is usually characterized by the chromatographic retention factor k' , which is defined in terms of experimentally observable quantities as

$$k' = \frac{t_r - t_{nr}}{t_{nr}} \quad 2.10$$

where t_r is the retention time of a solute under retentive conditions and t_{nr} is the retention time of that solute under non-retentive conditions. This operational definition of k' can be complemented by a mechanistic analysis of linear chromatography, which leads to the interpretation that

$$k' = K\phi \quad 2.11$$

Here K is an adsorption equilibrium constant that reflects the chemical character of the partitioning, and ϕ is the phase ratio that captures the physical character of the stationary phase, namely the available surface area per unit volume of mobile phase.

Chapter 3

MATERIALS AND METHODS

3.1 Materials

3.1.1 Adsorbents

Two strong cation exchanger adsorbents were studied, Toyopearl SP 650M and Toyopearl GigaCap 650M. Both adsorbents are manufactured by Tosoh Biosciences, and are based on the Toyopearl HW-65 size exclusion bead. Table 3.1 is a summary of the adsorbents' properties, as reported by the manufacturer. As can be seen, both adsorbents have similar properties, with a slight difference in mean particle size. GigaCap is also functionalized with secondary polymers of a composition that remains undisclosed by Tosoh Bioscience. These adsorbents were chosen to allow for an investigation into the effects of GigaCap's secondary polymers onto adsorption and mass transfer characteristics of the two adsorbent materials, with a specific focus on retention, capacity, and effective diffusivity.

Table 3.1: Resin properties for the two resins studied, as reported by the manufacturer^{36,37}

Resin	SP-650 M	GigaCap S-650 M
Manufacturer	Tosoh Bioscience	Tosoh Bioscience
Functional group	SO ₃ ⁻	SO ₃ ⁻
Mean particle size (μm)	65	75
Mean pore size (nm)	100	100*
Base matrix	PMMA	PMMA
Secondary polymers	None	Yes**

* This is the mean pore size associated with the 650M base matrix, and does not reflect the effective mean pore size of GigaCap upon inclusion of the secondary polymer layer

**The GigaCap adsorbent contains secondary polymers, which are of an undisclosed composition.

The adsorbents were kept in 20% ethanol for long-term storage, and were thoroughly cleaned before use by packing the desired amount of adsorbent into a 0.5 cm inner diameter column of variable height. The column was then sequentially washed with at least 10 column volumes of deionized water, at least 20 column volumes of 2 M sodium chloride, at least 10 column volumes of deionized water, and at least 20 column volumes of the desired equilibration buffer. Adsorbent quantities were measured using 200 μL WireTroll II capillaries (Drummond Scientific, Broomall, PA, USA). Adsorbent-buffer slurries were injected into the capillaries, and allowed to settle under gravity for a period of 30-60 minutes. The capillary's average height-to-volume ratio was 235 mm / mL, as determined by measuring the average height of the 100 μL marker for 10 capillaries. The relationship between the settled volume and the particle volume was determined from the column void fraction:

$$V_p = (1 - \epsilon) V \quad 3.1$$

where V_p and V are the particle volume and total volume, respectively, and ϵ is the void fraction. This void fraction was measured using a pulse response in a packed column. The columns were gravity packed with a known quantity of adsorbent, and 20 μL of a 1 mg / mL blue dextran solution was injected and eluted using water in up-flow and at a flow rate of 0.1 mL / min to minimize compression. Elution was monitored by absorbance at 280 nm. The blue dextran was obtained from Sigma, and was large enough (2000 kDa) to be completely excluded from the particle pores. Measured void fractions are reported in Table 3.2 for both adsorbents.

Table 3.2: Measured void fraction for adsorbents after settling under gravity

Adsorbent	Void Fraction
SP-650 M	0.408
GigaCap S-650 M	0.381

3.1.2 Columns

Waters AP minicolumns, 5 cm long x 0.5 cm i.d., were used in linear isocratic retention experiments. The columns were packed to a working height of 5 ± 0.5 cm using a 40% v/v adsorbent slurry and a packing solution of 1 M NaCl. Column packing quality was tested by measuring the band broadening of a 2% w/w acetone sample, with the eluent concentration monitored using UV absorbance at 280 nm. The

packing quality was evaluated using expressions for the inverse height of a theoretical plate³⁸

$$\frac{1}{HETP} = 5.54 \frac{\left[\frac{(t_{max} - t_0)}{(t_{50\%,2} - t_{50\%,1})} \right]^2}{L} \quad 3.2$$

and packing asymmetry

$$Y = \frac{t_{10\%,1} - t_{max}}{t_{max} - t_{10\%,2}} \quad 3.3$$

where t_{max} and t_0 are the elution times corresponding to maximum absorbance and the dead volume, respectively; L represents the column height; and $t_{50\%,1}$ - $t_{50\%,2}$ is the width of the peak at 50% maximum absorbance. Columns were used when $1/HETP$ was greater than 2500 meters, and the asymmetry was between 0.9 and 1.1.

3.1.3 Proteins

Experiments utilized the model proteins lysozyme and lactoferrin, the relevant physical and chemical properties of which are reported in Table 3.3. Both are globular proteins, and are positively charged in solutions of pH below 8.0. These proteins were chosen to allow investigation of the effect of protein size on the adsorption and mass transfer characteristics of the chosen adsorbent materials.

Thrice-crystallized hen egg white lysozyme was purchased from Sigma Aldrich (St. Louis, MO), and was not purified further before use. Lyophilized lactoferrin was kindly donated by DMV-International (Veghel, The Netherlands). The lactoferrin was

further purified by ion-exchange chromatography using a 1.6 cm i.d x 20 cm long XK 16 column (GE Healthcare) packed with SP Sepharose FF. Figure 3.1 is the chromatogram of a typical lactoferrin purification. Lactoferrin eluted in the peak corresponding to fractions G3 to I2, and fractions G6 to H10 were recovered for experimental use.

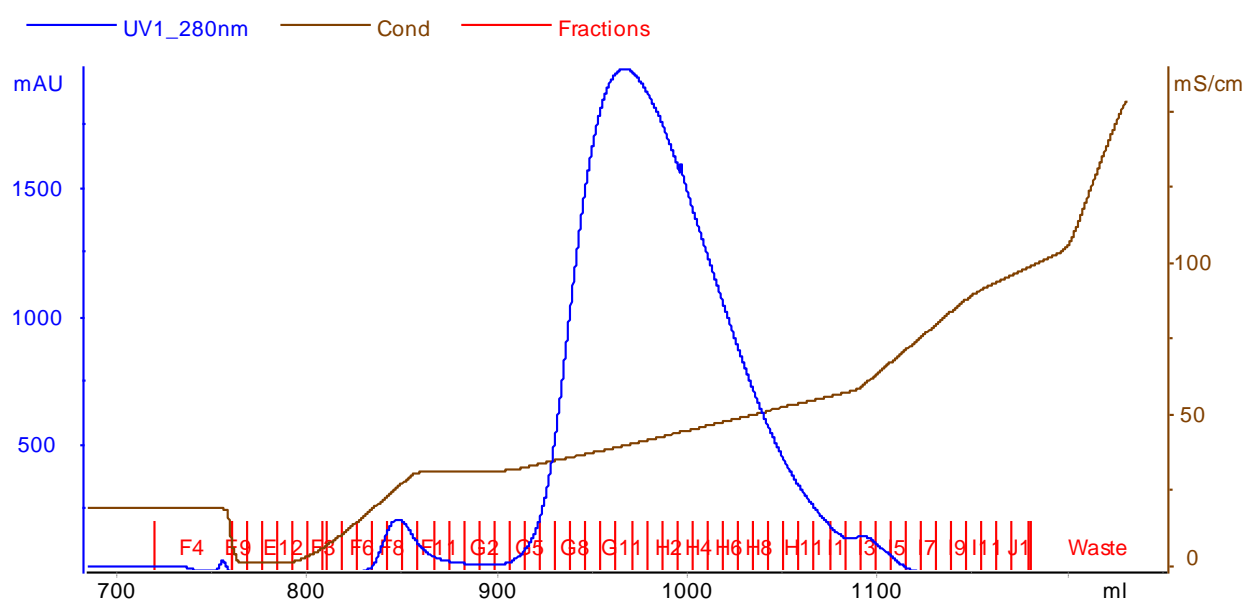


Figure 3.1: Representative run from a separation of lactoferrin using Sepharose FF. Elution was monitored using absorbance at 280 nm (blue), and elution was performed using ionic strength (brown).

Protein concentrations were measured using absorbance at 280 nm, which was measured using a PharmaSpec UV-1700 (Shimadzu Corporation, Kyoto, Japan).

Solution concentrations were calculated using Beer's law:

$$A = \epsilon l C$$

3.4

where ϵ is the extinction coefficient given in Table 3.3, l is the path length (1 cm), A is the absorbance and C is the solution concentration.

Table 3.3: Relevant physicochemical properties of the two proteins used in this study¹¹.

Property	Lysozyme	Lactoferrin
Molecular weight (kDa)	14.3	78
Isoelectric pH	11.3	8.0-9.5
Effective molecular radius (nm)	1.6	2.7
Net charge at pH 7	+8	+16
Diffusion coefficient (cm ² /s)	1.12 x 10 ⁻⁶	0.96 x 10 ⁻⁶
Extinction coefficient (cm ² /mg)	2.64	1.51

3.1.4 Buffer Solutions

Buffer solutions were prepared using ACS grade chemicals obtained from Fisher Scientific (Fair Lawn, NJ). 10 mM monosodium phosphate was used to provide buffering at a pH of 7.0 ± 0.1. The pH was adjusted by addition of NaOH, and the ionic strength was adjusted by addition of NaCl. Buffers with ionic strengths below 20 mM were prepared by dilution of a 10 mM phosphate buffer with deionized water. All

buffers were degassed using helium, and filtered through a 0.22 μm cellulose-acetate membrane before storage.

3.2 Methods

3.2.1 Isotherm Determination

Adsorption isotherms were determined by measuring the equilibrium batch uptake of protein onto each adsorbent. Samples of a stock solution of protein were added to Fisher brand 1.5mL microcentrifuge vials (Eppendorf AG, Hamburg, Germany). The adsorbent was measured using WireTroll capillaries as described earlier, and injected into the vials. The samples were continuously rotated for equilibration periods of a minimum of 1 day for lysozyme, and 3 days for lactoferrin. This difference in equilibration periods represents the difference in mass transfer rates for the two proteins, and was verified by in lab. The adsorbed protein concentrations could not be measured directly, and were instead calculated from a mass balance:

$$q = (C_0 - C^*) \frac{V_{sol}}{V_{ads}} \quad 3.5$$

where C_0 and C^* are the initial and final solution concentration, respectively, and V_{sol} and V_{ads} are the volume of liquid and adsorbent, respectively.

Adsorption isotherms were fitted to the colloidal model discussed in chapter 2 (Eqn. 2.2). This equation was transformed to the form³³

$$\ln\left(\frac{\phi C^*}{q^*}\right) - \ln K_{eq} + B_{pp} \left(\sqrt{q^*} + \beta \right) \exp\left(\frac{\omega}{\sqrt{q^*}}\right) \quad 3.6$$

allowing the interaction parameters, K_{eq} and B_{pp} , to be obtained from a linear fit. The phase ratios used in the fits are shown in Table 3.4. The phase ratio of SP-650M has been reported by DePhillips and Lenhoff¹⁶ for several different dextran probes sizes, as determined through inverse size-exclusion chromatography (ISEC). The reported values for lysozyme and lactoferrin were calculated from a linear extrapolation, based on each protein's effective molecular radius reported in Table 3.3. The phase ratios for GigaCap have not been reported or measured, and were estimated by comparison to Sepharose FF and Sepharose XL. This estimate is not representative of the actual GigaCap phase ratio, and thus should not be used in a mechanistic interpretation. Instead, it is merely used in the context of fits using the colloidal model.

Table 3.4: Phase ratios used in the fits of isotherm data to the colloidal isotherm model.

Adsorbent	ϕ (m ² /mL)	
	Lysozyme	Lactoferrin
SP-650M ¹⁶	22.9	20.6
GigaCap	52	47

3.2.2 Batch Uptake

Dynamic batch adsorption experiments were used to quantify protein uptake as a function of time. Figure 3.2 is a schematic of the experimental setup used.

Experiments were performed in a baffled 150 mL beaker. 100 mL of 3 ± 0.2 mg/mL of protein were poured into a 150 mL flask. The bulk solution was continuously drawn through a 10 μ m stainless steel filter (Upchurch Scientific, Model A302) using an Äkta P960 pump. The absorbance of the filtered solution was measured using an Äkta UV Cell 2 at 280 nm, and returned to the beaker. The extraneous volume associated with the tubing and flow cell was less than 2.2 mL. The slurry was mixed using agitation from a T-Line Laboratory Stirrer that was equipped with a 3-bladed impellor. A baseline was first established, and adsorbent was then measured and injected into the solution. The bulk solution absorbance measured after injection of the adsorbent was used to construct a protein uptake curve as a function of time.

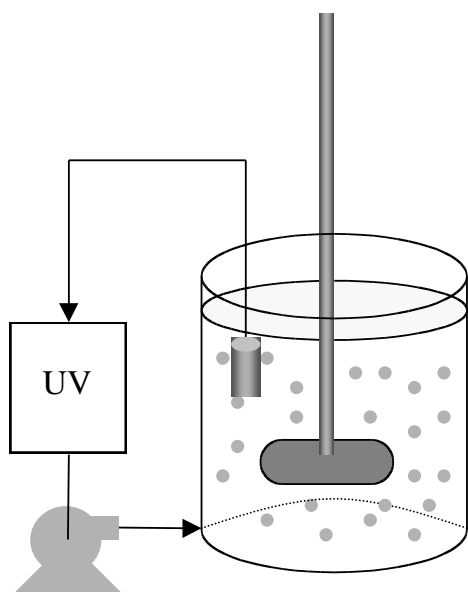


Figure 3.2: Schematic of experimental apparatus used in batch uptake experiments. Device included a UV cell, peristaltic pump, beaker, and 3-bladed impeller.

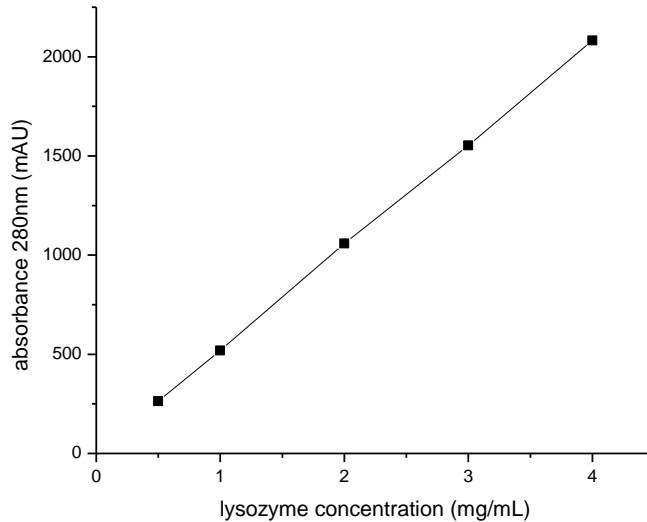


Figure 3.3: Calibration of the Äkta UV flow cell for different lysozyme concentrations. The plot shows a linear dependence with $R^2=0.9998$ and slope of 520.81 mAU.mL/mg.

The Äkta UV cell was calibrated using lysozyme, as shown in Figure 3.3. This allowed for calculation of the bulk solution's protein concentration using $A = bC \frac{e_p}{e_{lys}}$.

Estimates of the effective diffusivity were obtained by fitting the uptake data to the shrinking core model. The Matlab nonlinear regression function `nlinfit` was used to regress the uptake curve over the effective pore diffusivity, using a final saturation plateau obtained from the isotherm experiments. The mass transfer coefficient related to transfer from the bulk solution was estimated using correlations provided by

Armenante and Kirwan (1989) for the Sherwood number³⁹, and Sano and Usui (1985) for impeller power input⁴⁰. The error associated with the fitted D_e was estimated using the Matlab function `nlinparci`, using the covariance matrix returned by `nlinfit`.

3.2.3 Isocratic Retention

Pulse response experiments were used to measure adsorption under isocratic conditions, and these results were used to calculate the retention factor, k' . Waters minicolumns of 0.5 cm i.d. were packed to heights of 5 ± 0.5 cm, as described earlier. The chromatography experiments were performed using a Waters 2695 chromatography workstation, with a Waters 2996 photodiode array detector used to monitor eluate absorbance at 280 nm. Twenty μL injections of solutions of protein concentration 1-5 mg/mL were used, and eluted with a buffer of the same ionic strength at a flow rate of 0.2 mL/min. Retention times were determined for both proteins, on both adsorbents, and over a range of ionic strengths. The eluent ionic strength was between 200 mM and 2 M ionic strength, and was controlled by the mixing of 10 mM phosphate buffers at 20 mM, 1 M or 2 M ionic strength. Mixing was performed inline during runs, by parallel injection of a high salt and a low salt buffer in a predetermined ratio. The column was washed with 5 column volumes of 2 M ionic strength buffer, 2 column volumes of water and 10 column volumes of the elution buffer between runs. The system's extra-column volume was 0.613 mL, as determined by injection of an acetone tracer with the column taken out of line.

The retention time was calculated using the ratio of the first and zeroth moments of the elution peak

$$t_r + t_0 = \frac{\int C \overline{t} dt}{\int C dt} \quad 3.7$$

Where t_r and t_0 are the retention times due to the column and extracolumn effects, respectively. The retention factor, k' , was then calculated from Eqn 2.11.

Chapter 4

RESULTS AND DISCUSSION

This chapter describes the results obtained from the adsorbent characterization experiments. Results are obtained at pH 7.0 and for several ionic strengths, and represent characterization of the bulk transport, adsorption, and retention properties for lysozyme and lactoferrin onto SP-650M and GigaCap.

4.1 Isocratic Pulse Response

Figure 4.1 is a log-log plot of the normalized retention factor (k') versus ionic strength for lactoferrin and lysozyme on SP-650M, and for lysozyme on GigaCap. Retention results could not be calculated for lactoferrin on GigaCap, as explained later in this section. These results display a linear relation when plotted in log-log form. The k' data thus have a power-law dependence on ionic strength, which is consistent with the stoichiometric displacement model^{21,41}. This plot shows pronounced retention differences for different combination of protein and adsorbent, which are especially significant given the log-log form of the data representation. Specifically, lactoferrin displays much higher retention on SP-650M than lysozyme does on either adsorbent, and lysozyme displays much higher retention on GigaCap than on SP-650M.

Each log-log data set shows good agreement with a linear fit, with fit parameters given in Table 4.1. This linear behavior allows for quantitative comparisons between the retention behavior of each protein and adsorbent pair. The retention plots for lysozyme on SP-650M and for lysozyme on GigaCap are nearly parallel, with a typical retention difference of about a factor of 6. Such large differences in retention between the two adsorbents are probably due to more than just an increased accessible surface area for GigaCap, and imply increased interactions for GigaCap, which may initially be attributed to electrostatics.

Alternatively, the slope of lactoferrin retention on SP-650M is much steeper than that of lysozyme retention on SP-650M, with typical retention differences between a factor of 10 and 100. These retention differences are presumably due primarily to differences in the associated adsorption energetics, i.e. electrostatics. They are presumably a result of the combination of the much greater net charge of lactoferrin than lysozyme at pH 7, as well as the highly uneven charge distribution in lactoferrin. Significantly, the charge effects between lysozyme and lactoferrin are clearly stronger than the adsorbent effects between SP-650M and GigaCap, as the lactoferrin-SP-650M pair also exhibits greater retention than the lysozyme-GigaCap pair.

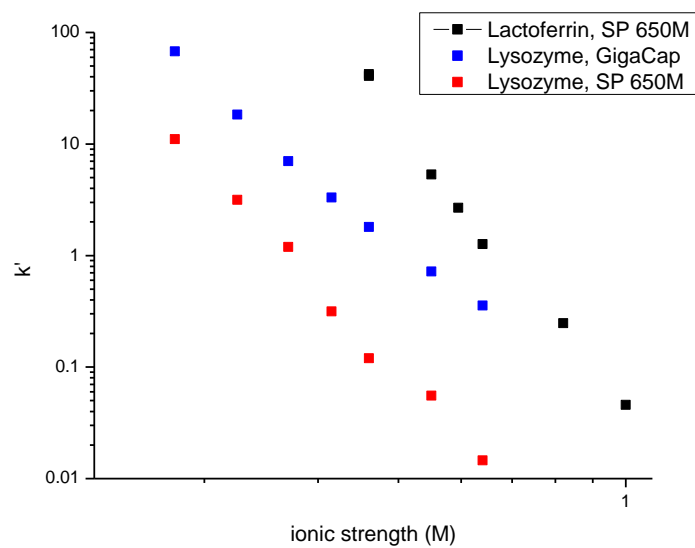


Figure 4.1: k' data for lysozyme on SP-650 M (red), lysozyme on GigaCap (blue), and lactoferrin on SP 650-M (black). Results were collected from pulse response of solute at pH 7.0. GigaCap-lactoferrin results were not included, as their elution behavior precluded k' analysis.

Table 4.1: Parameters obtained from a fit of k' data to $\ln(k') = m * \ln(IS) + b$

Adsorbent	Protein	m	b	R2
SP 650 M	Lysozyme	-4.7	-5.3	0.998
SP 650 M	Lactoferrin	-7.3	-3.2	0.991
GigaCap	Lysozyme	-4.5	-3.3	0.994

Figure 4.2 shows the experimental chromatograms obtained from pulse responses of lactoferrin on GigaCap at two different salt strengths. This figure also shows plots of lactoferrin on SP-650M and lysozyme on GigaCap, both under non-retaining conditions. As can be seen, the lactoferrin-GigaCap elution occurs in highly

asymmetric peaks, with the peak maxima and first moments corresponding to about 35 and 45% of a column volume, respectively, and with extensive peak tailing that is present beyond one column volume. It is the asymmetric nature of these peaks that prevent the analysis shown in Figure 4.1. Conversely, the unretained elution peaks for lysozyme on GigaCap, and lactoferrin on SP-650M, correspond to about 65% and 75% of a column volume, respectively. In addition, the peak tailing observed for the unretained elution of lysozyme on GigaCap, and lactoferrin on SP-650M, is much less pronounced, and can be attributed mostly to extra-column effects.

This elution behavior of lactoferrin on GigaCap is not typical for retained k' measurements in the linear and weakly retained region, which tend to give fairly symmetrical peaks. It was not replicated for lactoferrin on SP-650M, or for lysozyme on either SP-650 M or GigaCap. It is also not an artifact of the column packing, as packing tests with an 2% w/w acetone tracer eluted in roughly 85% of the column volume, and with a 95% symmetric peak.

The early elution is evidence that lactoferrin is excluded from a larger portion of the GigaCap adsorbent matrix than seen from lactoferrin on SP-650M, or lysozyme on GigaCap. The fact that elution occurs after the column void volume ($V_0 \sim 35\%$ of a column volume) suggests that the lactoferrin is able to penetrate the adsorbent matrix, but that the effects represent exclusion from a large fraction of the pore volume. Inverse size exclusion chromatography (ISEC) measurements of the SP-650M base matrix, upon which GigaCap is based, have been performed by DePhillips and

Lenhoff¹⁶, and suggest that small-radius pores comprise a relatively small fraction of the entire pore volume. In addition, lactoferrin eluted after one column volume on the SP-650M material, which should have a similar pore structure to GigaCap, apart from the polymer modifier. It is thus extremely unlikely that the observed lactoferrin exclusion is due to exclusion from the smaller particle pores, and thus suggests exclusion from the GigaCap polymer layer. This exclusion is presumably due to the protein size, as lysozyme showed more access to the GigaCap adsorbent structure.

The elution profiles of lactoferrin on GigaCap are also notable due to the presence of significant tailing. The magnitude of this tailing is greater for the lower ionic strength pulse experiment, which indicates a sensitivity to electrostatic interactions. As the tailing is greater for the pulse at lower ionic strength, it appears likely that this tailing is due to attractive electrostatic interactions between the protein and the adsorbent. If so, these attractions are much weaker than would be expected, as they do not lead to significant retention inside the particle, which was observed for lactoferrin-SP-650M at 700mM ionic strength. This may thus indicate that, while the electrostatic forces are still present, the polymer layer presents a steric hindrance that significantly reduces lactoferrin's ability to adsorb. Another possible explanation is that the tailing reflects slow egress of the protein from the polymer layer, which may be aggravated by contraction of the polymer layer at higher salt. Such conformational changes would be due to the additional electrostatic screening of the ion-exchange ligands attached to the polymer layer, as low-salt conditions would promote extended

polymer conformations in an attempt to reduce the strength of ligand-ligand repulsion¹⁶.

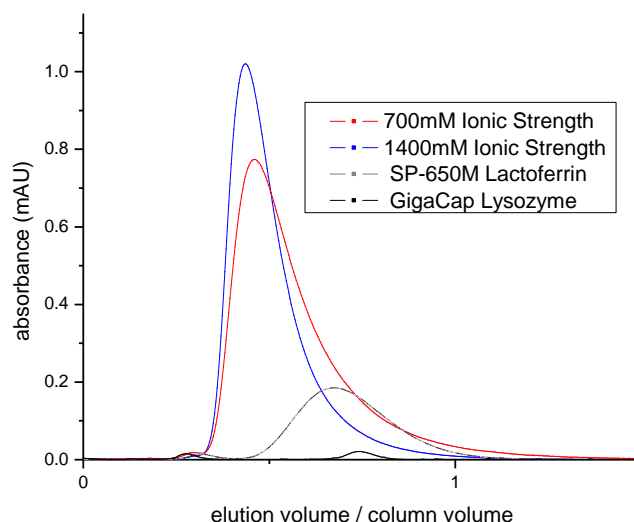


Figure 4.2 Elution profiles from isocratic pulse response experiments of lactoferrin on GigaCap. The blue and red lines correspond to isocratic pulses at 1400mM and 700mM ionic strength, respectively. Elution profiles for unretained pulses of lactoferrin on SP-650M (black) and lysozyme on GigaCap (gray) are also shown for comparison.

4.2 Adsorption Isotherms

Adsorption isotherms for lysozyme on GigaCap, and lactoferrin on both SP 650M and GigaCap are shown in Figure 4.3-4.5 for ionic strengths between 2mM and 200mM, and at pH 7.0. Solid lines are the fits to the colloidal model using the phase

ratios reported in Table 3.4. All isotherms display the concave-downward shape that is typical for strong ion-exchangers, although the isotherms differ in capacity and initial slope. All isotherms also display the trends of increasing capacity and increasing rectangularity with decreasing ionic strength that are expected for strong ion-exchangers²⁰.

The equilibrium adsorption isotherm data demonstrate that GigaCap has a very high capacity for lysozyme, with static capacities approaching 300mg/mL of resin. In addition, these isotherms are all near-rectangular, and show little softening at higher salt concentrations. The isotherms also show a very high initial slope, again with very little variation in salt strength, which suggests that the high capacities are mainly due to strong protein-adsorbent interactions²⁰.

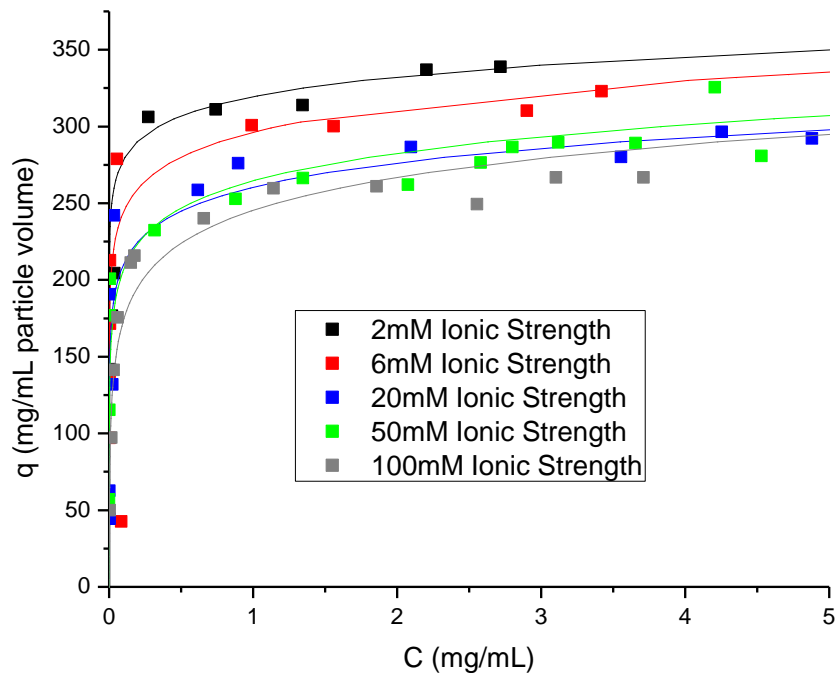


Figure 4.3: Adsorption isotherms for lysozyme on GigaCap at 2 mM (black), 6 mM (red), 20 mM (blue), 50 mM (green) and 100 mM (gray) ionic strengths. Points are experimental data, and lines are fits to the colloidal model.

Adsorption isotherms for lactoferrin on GigaCap also display very high static capacities, which approach 280 mg/mL at 20 mM ionic strength. While rectangular at low ionic strengths, these isotherms show significant softening at higher ionic strengths, and are less rectangular than the lysozyme isotherms. This softening may be indicative of weaker protein-adsorbent interactions, and may be due to surface area effects. In addition, there may be a contribution due to the stronger protein-protein interactions for lactoferrin than lysozyme, which may be explained by the higher net

charge and charge asymmetry of lactoferrin. However, it is unlikely that protein-protein interactions comprise the full contribution to the softening behavior, due to the low protein concentrations found in this region.

In addition, the static capacities show a substantial reduction with increasing ionic strength. This trend of decreasing capacity with increasing salt strength may be explained by decreases in the strength of the attractive protein-surface interactions, which is supported by the shallow initial slopes observed at higher ionic strengths. However, decreasing protein-surface interactions may not be enough to explain the substantial capacity reductions observed. In addition, these reduced capacities are probably not a result of protein-protein interactions, which should be smaller for the higher ionic strength conditions. Decreasing electrostatic interactions may thus be adequate to explain only a portion of this behavior. The observed capacity decreases may thus represent an initial stage of the exclusion effects initially observed in the lactoferrin-GigaCap k' data, as explained by conformational shrinkage of the GigaCap polymer layer at higher ionic strengths as well as possibly other exclusion mechanisms.

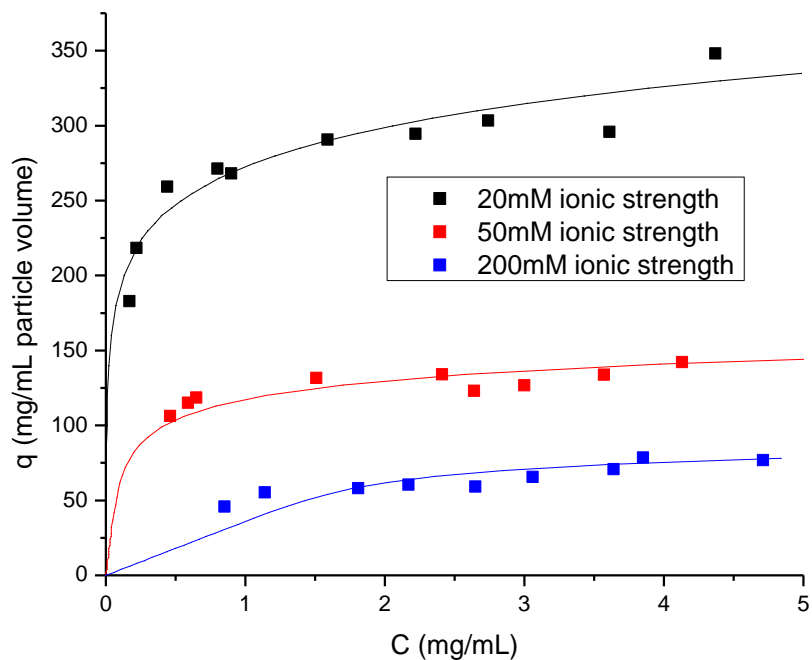


Figure 4.4: Adsorption isotherms for lactoferrin on GigaCap at 20 mM (black), 50 mM (red) and 200 mM (blue) ionic strength. Points are experimental data, and lines are fits to the colloidal model. Note that colloidal model fits are worse at high ionic strengths.

The adsorption isotherms for lactoferrin on SP 650 display relatively low static capacities, which approach 95 mg/mL at low ionic strength. These isotherms show consistently low capacity for lactoferrin, which are in agreement with the low capacity for lysozyme observed by Dziennik¹¹. These isotherms are also fairly soft, with capacity changes of about 30% between bulk solution concentrations of 1 mg/mL and 4 mg/mL.

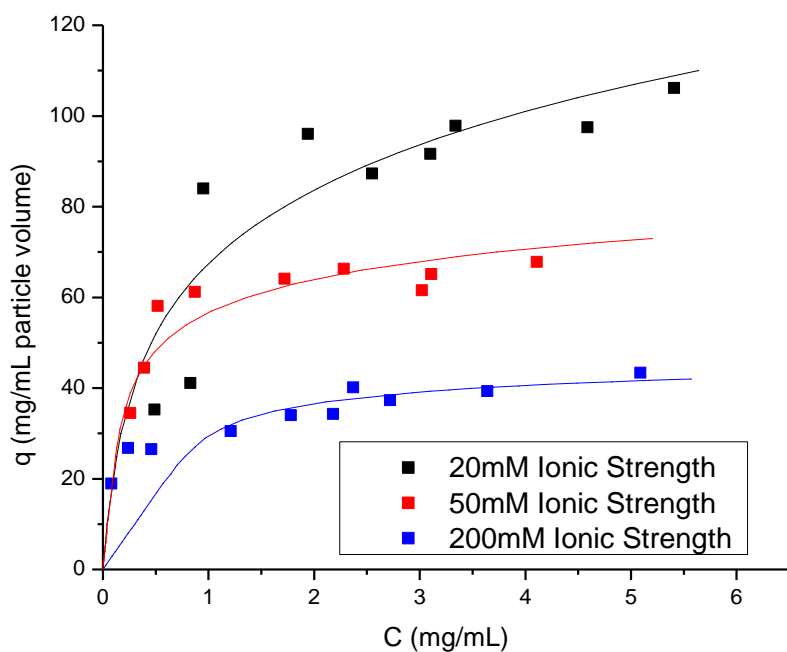


Figure 4.5: Adsorption isotherms for lactoferrin on SP 650 M at 20 (black), 50 mM (red), and 200 mM (blue) ionic strength, pH 7. Points are experimental data, and lines are fits to the colloidal model.

It is also worth noting that the colloidal model provides fairly poor fits to the lactoferrin isotherms onto both GigaCap and SP-650M. Although the fits give an adequate representation of the observed trends, they are not suitable for mechanistic interpretation. This may indicate that the colloidal model provides a mechanistically unsuitable description of adsorption for either large proteins, or proteins with extremely asymmetric charge distributions.

The static capacities of both lysozyme and lactoferrin on both GigaCap and SP-650 M are reported in Figure 4.6 and Figure 4.7. All capacities are estimated from the isotherm plateaus, except for those of lysozyme on SP-650 M, which are estimated from the batch uptake data shown in the next section. Again, all plots show the same trend of decreasing capacity with increasing ionic strength. However, GigaCap shows much more substantial decreases in static capacity between low and moderate ionic strengths than SP-650 M. While this behavior is observed for both proteins, it is much more pronounced for lactoferrin than lysozyme. Interestingly, GigaCap's lysozyme capacity is consistently more than 3 times greater than SP-650M's lysozyme capacity, whereas GigaCap's lactoferrin capacity changes from nearly 3 times SP-650M's lactoferrin capacity to less than double. Such a significant reduction in static capacity is usually observed only for much larger modulations in salt strength, and may be additional evidence of exclusion effects from the secondary-polymer layer at high salt strengths. These effects are also similar to those observed by Bowes et al.²⁸ for mAb and lactoferrin adsorption onto the dextran-modified adsorbents Q Sepharose XL and

Capto Q. While not fully understood, they may serve as additional evidence that the secondary-polymer layer experiences subtle changes in structure due to changing salt strength. These structural changes may increase the steric barrier to adsorption, which is compounded by the reduction in electrostatic driving forces for adsorption seen at higher salt strengths.

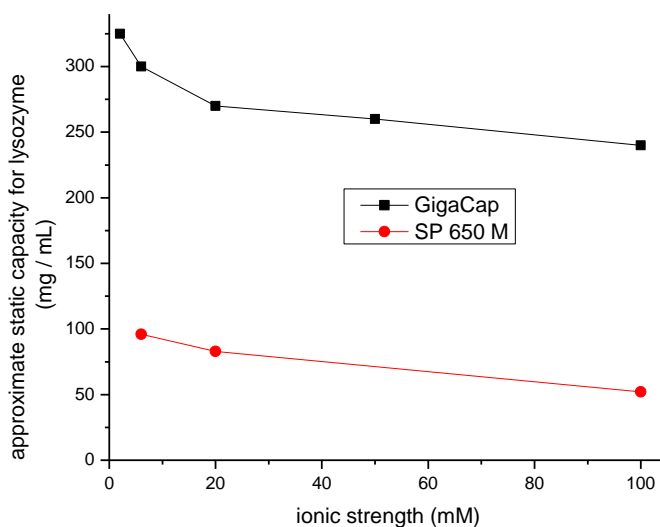


Figure 4.6: Variation of static capacities with ionic strength for lysozyme on GigaCap and SP 650M. Capacities on GigaCap were estimated from isotherm plateaus, and capacities on SP-650M were estimated from batch uptake data.

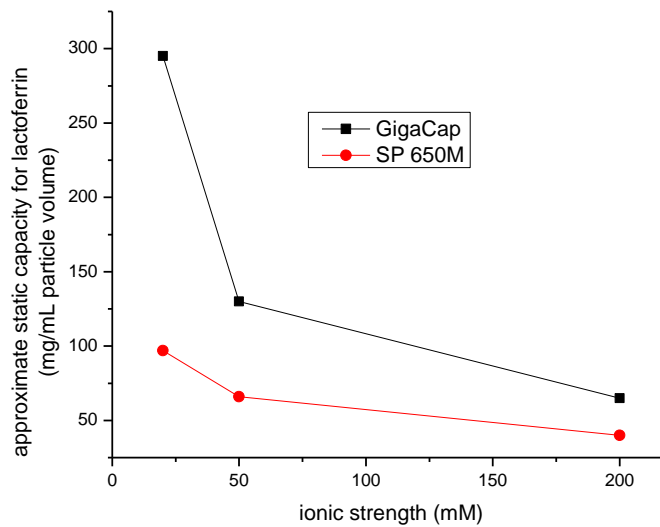


Figure 4.7: Variation of static capacities with ionic strength for lactoferrin onto GigaCap and SP 650M. All capacities were estimated from the isotherm plateaus.

4.3 Batch uptake

Figure 4.8-Figure 4.11 show the results of batch uptake experiments conducted for lysozyme and lactoferrin adsorption onto SP-650M and GigaCap . Data are reported in terms of an average adsorbed protein concentration vs. time; the dashed lines are experimental data and the solid lines are fits to the shrinking core model. Experiments for each protein-adsorbent pair show the trend of increased equilibration time with decreasing ionic strength. They also show significantly increased initial uptake rates, but much longer ultimate equilibration times, for GigaCap relative to SP-650 M.

In general, the shrinking core model fits the experimental data poorly. The fits consistently show a slight underprediction of uptake rates for the initial portions of the curve, and a large overprediction of uptake in the final portions of the curve. This kind of bimodal behavior is also often apparent in column breakthrough experiments, and cannot be readily explained by most simple transport and kinetic models⁴²; therefore models other than the shrinking core model are also unlikely to capture the bimodal behavior. This performance may indicate that pore diffusion is dominant during the initial stages of uptake, and quickly achieves partial saturation in most of the particle volume, but that additional adsorption is necessary to achieve full particle equilibration. Although not entirely consistent with the shrinking core model, it is consistent with the observed behavior that adsorbents quickly saturate to a substantial fraction of their full saturation capacity, and then approach full saturation at a much lower rate. This slow step may reflect the small residual amount of surface area available⁴³, or rearrangement mediated by surface diffusion. An alternative explanation is that this behavior may be evidence of significant heterogeneity with respect to particle size. Such heterogeneity typically results in both faster initial uptake behavior, as well as slower equilibration behavior, than predicted by the shrinking core model²². However, invoking these effects would only account for a portion of the tailing observed experimentally. Although models have been developed to account for the effects of particle size distribution on shrinking core uptake²⁷, size distribution effects were not included in the fits due to the lack of necessary size distribution data.

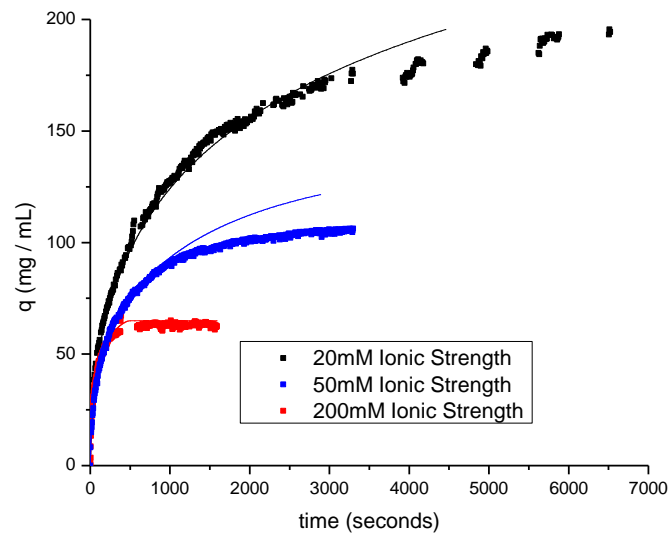


Figure 4.8: Lactoferrin uptake on GigaCap for solution pH 7.0 and ionic strengths of 20 mM (black), 50 mM (blue), and 200 mM. Solid lines are fits to the shrinking core model.

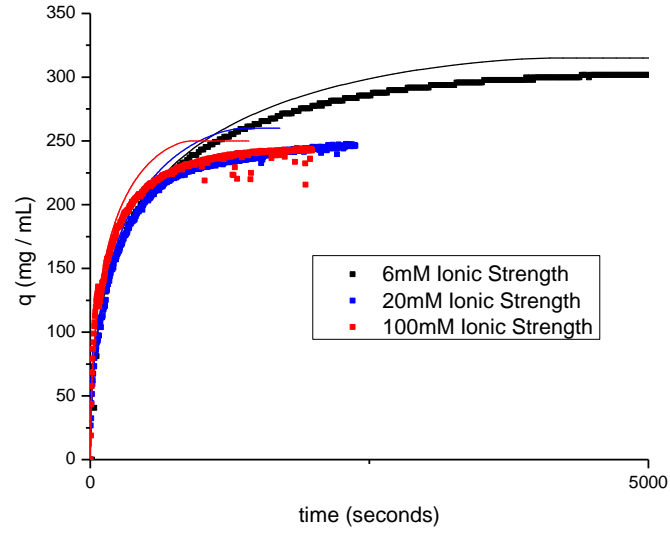


Figure 4.9: Lysozyme uptake on GigaCap for solution pH 7.0 and ionic strengths of 6 mM (black), 20 mM (blue), and 100 mM (red). Solid lines are fits to the shrinking core model.

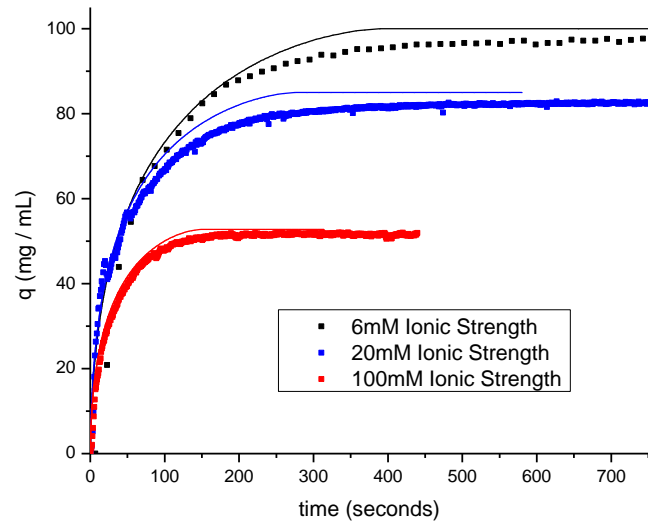


Figure 4.10: Lysozyme uptake onto SP-650 for solution pH 7.0 and ionic strengths of 6 mM (black), 20 mM (blue), and 100 mM (red). Solid lines are fits to the shrinking core model.

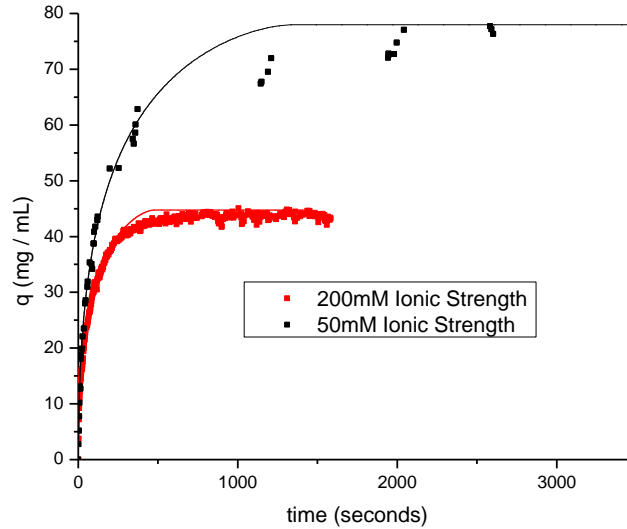


Figure 4.11: Lactoferrin uptake onto SP-650M for solution pH 7.0 and ionic strengths of 20 mM (black), 50 mM (blue), and 200 mM. Solid lines are fits to the shrinking core model.

Figure 4.12 is a summary of the normalized effective diffusivities (D_e/D_0) obtained from the fits of the shrinking core model to the batch uptake data. All proteins show an increase in the effective pore diffusivities with increases in ionic strength. The normalized effective diffusivity of lactoferrin on GigaCap is consistently greater than that of lactoferrin on SP-650 M, and consistently less than that of lysozyme on either adsorbent. Interestingly, this consistency is not observed for the normalized lysozyme diffusivities, the differences between which are only statistically significant at 100 mM ionic strength.

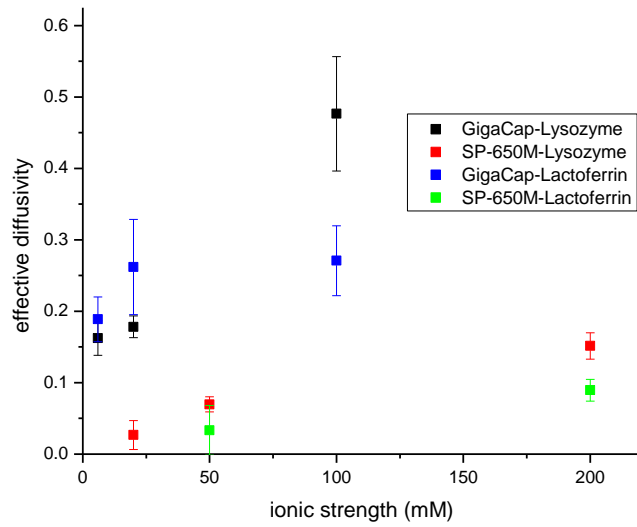


Figure 4.12 The effect of ionic strength on the normalized effective diffusivity, as fit to the shrinking core model, (D_e/D_0) of lysozyme and lactoferrin on GigaCap and SP 650M. Error bars are the 95% confidence interval.

Chapter 5

CONCLUSIONS AND IMPLICATIONS

The results presented in this thesis have several important implications regarding the effects of secondary polymers on an adsorbent's chromatographic performance. Isocratic retention experiments showed that lysozyme was much more strongly retained on GigaCap than on SP-650M, and that lactoferrin had much higher retention on SP-650M than lysozyme on GigaCap. This implies that, although the secondary polymers may contribute increased retention due to a combination of increased surface area and ligand accessibility, such retention is outweighed by the increased electrostatic attraction that may be associated with a different protein. Retention experiments for lactoferrin on GigaCap also demonstrated minimal retention at higher salt, as well as partial exclusion from the GigaCap adsorbent matrix. This implies some mechanism of lactoferrin exclusion from the polymer layer that was not observed in either lysozyme retention on GigaCap, or lactoferrin retention on SP-650M.

Isotherm determination for lysozyme and lactoferrin successfully showed that, given the same solution ionic strength and pH, GigaCap possessed greater retention and static capacities than SP-650M. Importantly, these capacity differences were

substantially reduced for lactoferrin, the larger protein. These observed capacity differences were substantially decreased upon increasing ionic strength, behavior that was much more pronounced for lactoferrin than lysozyme. When coupled with the partial exclusion observed in the lactoferrin-GigaCap retention experiments, one possible interpretation may be that the conformation of GigaCap's polymer layer depends on ionic strength. Whether caused by conformational changes¹⁶, lack of an electrostatic driving force for adsorption^{22,44}, or some alternative mechanism, this effect contributes to particle exclusion at high to moderate ionic strengths, and significantly decreases the capacity and retention behavior.

Batch uptake experiments showed the general trend of increasing pore diffusivity with decreasing ionic strength for all combinations of protein and adsorbent. In addition, while the proteins sometimes displayed increased mass transfer for GigaCap relative to SP-650, such differences were small, and not always statistically significant. In addition, the shrinking core model showed poor fits to the experimental data, and consistently under-predicted both initial transport and adsorption rates, as well as final equilibration times. While these fits were poor for all protein and adsorbent combinations, the performance was worse for lactoferrin uptake than lysozyme uptake.

Altogether, these experimental results may demonstrate that significantly higher capacities, as well as potentially increased mass transport rates, may be obtained via polymer modification of existing resins. However, exclusion effects are

observed that may be related to sensitivity of the polymer layer's conformation to ionic strength, and increase with solute size. Such conformational changes are most likely a result of polymer shrinkage at high ionic strength, due to the reduction of ligand-ligand repulsion. If true, such shrinkage would decrease the accessibility of large molecules for the polymer layer, effectively increasing the steric barriers to adsorption. This steric effect may be coupled with an additional electrostatic effect, where salt screening reduces the strength of the electrostatic force necessary to drive protein adsorption into the polymer layer. However, the exclusion effect is much more pronounced for lactoferrin than lysozyme. Lactoferrin has both a higher net charge, and a larger effective molecular radius than lysozyme, which implies that the exclusion effects are dominated by the steric effects.

The exclusion behavior is observed for ionic strengths that are relevant for chromatographic process operations. Thus, they may potentially serve as a limitation on the effectiveness of polymer-modified media in preparative separations processes, especially given the prominence of high-molecular weight products, such as mAbs and DNA vaccines. Unintentional ionic strength deviations during operation may potentially result in drastic changes in process performance, and serve to limit process efficiency, robustness, and product quality. It is thus important that these conditions be recognized in chromatographic operations design, during both step optimization and preliminary adsorbent screening.

These observed exclusion effects are also relevant to future resin design, as it may be desirable to either reduce or exploit these effects in future adsorbents. Specifically, this presents an opportunity to design ion-exchange resins that have a high affinity for proteins of a specific molecular size range. Alternatively, it may be desirable to incorporate a possible reduction of this behavior into future adsorbents, which may be necessary for the design of adsorbents with robust, high capacities for larger macromolecules such as mAbs.

REFERENCES

1. Yang, C. Shyu, J. Cross-national and cross-industrial comparison of two strategy approaches for global industrial evolution. *Technological Forecasting and Social Change* 76, 2-25 (2009).
2. Venter, J.C. et al. The sequence of the human genome. *Science* 291, 1304-1351 (2001).
3. RCSB Protein Data Bank. <<http://www.rcsb.org/pdb/home/home.do>>
4. Strategic Consulting Report. Biopharmaceuticals: Current market dynamics & future outlook. ASInsights (2005).
5. Market Research Group. Biotech 2008 Life Sciences: A 20/20 Vision to 2020. (2008).
6. Moulds, J. Pfizer buys Wyeth for \$68bn. *Telegraph.co.uk* (2009).
7. Kalyanpur, M. Downstream processing in the biotechnology industry. *Molecular Biotechnology* 22, 87-98 (2002).
8. Rathore, A.S.; Latham, P.; Kaltenbrunner, O.; Curling, J.; Levine, H. Costing Issues in the Production of Biopharmaceuticals. *Biopharm International* (2004).
9. Langford, J.F.; Xu, X.K.; Yao, Y; Maloney, S.F.; Lenhoff, A.M. Chromatography of proteins on charge-varient ion exchangers and implications for optimizing protein uptake rates. *Journal of Chromatography A*, 1163, 190-202 (2007).
10. Trilisky, E.I.; Lenhoff, A.M. Sorption processes in ion-exchange chromatography of viruses. *Journal of Chromatography A*. 1142, 2-12 (2007).
11. Dziennik, S.; Belcher, E.B.; Barker, G.A.; Lenhoff, A.M. Nondiffusive mechanisms enhance protein uptake rates in ion exchange particles 100, 420-425 (2003)

12. Pabst, T. pH Transitions, Protein Separations, and Mass Transfer in Chromatography Columns Containing Weak Ion Exchange Groups, Ph.D. thesis, University of Virginia, Charlottesville, 2008.
13. DePhillips, P.; Lenhoff, A. Determinants of protein retention characteristics on cation-exchange adsorbents. *Journal of Chromatography A*. 933, 57-72 (2001).
14. Xu, X. Protein adsorption isotherms and their effects on transport in cation-exchange chromatography, Ph.D. thesis, University of Delaware, Newark (2008).
15. Ladiwala, A.; Rege, K.; Breneman, C.M.; Cramer, S.M. A priori prediction of adsorption isotherm parameters and chromatographic behavior in ion-exchange systems. *Proceedings of the National Academy of Sciences of the United States of America* 102, 11710-11715 (2005).
16. DePhillips, P.; Lenhoff, A.M. Pore size distributions of cation-exchange adsorbents determined by inverse size-exclusion chromatography. *Journal of Chromatography A*. 883, 39-54 (2000).
17. DePhillips, P. et al. Effect of spacer arm length on protein retention on a strong cation exchange adsorbent. *Analytical Chemistry* 76, 5816-5822 (2004).
18. Dziennik, S.D. Belcher, E.B. Barker, G.A. Lenhoff, A.M. Effects of ionic strength on lysozyme uptake rates in cation exchangers. I: Uptake in SP Sepharose FF. *Biotechnology and Bioengineering* 91, 139-153 (2005).
19. Hunter, A.; Carta, G. Protein adsorption on novel acrylamido-based polymeric ion-exchangers I. Morphology and equilibrium adsorption. *Journal of Chromatography A* 897, 65-80 (2000).
20. Oberholzer, M.R. Lenhoff, A.M. Protein adsorption isotherms through colloidal energetics. *Langmuir* 15, 3905-3914 (1999).
21. Brooks, C.A. Cramer, S.M. Steric mass action ion-exchange-displacement profiles and induced salt gradients. *AIChE J.* 39, 538-538 (1993).
22. Hunter, A.; Carta, G. Protein adsorption on novel acrylamido-based polymeric ion exchangers II. Adsorption rates and column behavior. *Journal of Chromatography A* 897, 81-97 (2000).
23. Schirmer, E.B. & Carta, G. Protein adsorption kinetics in charged agarose gels: Effect of agarose content and modeling. *AIChE J.* 55, 331-341(2009).

24. Hubbuch, J. et al. Dynamics of protein uptake within the adsorbent particle during packed bed chromatography. *Biotechnology and Bioengineering* 80, 359-368 (2002).
25. Stone, M.C. & Carta, G. Protein adsorption and transport in agarose and dextran-grafted agarose media for ion exchange chromatography. *Journal of Chromatography A* 1146, 202-215 (2007).
26. Karlsson, E. Rydén, L. Brewer, J. Ion Exchange Chromatography. Section 4 in J. Janson and L. Ryden (Ed.); *Protein Purification*. (Wiley-VCH: New York, 1998).
27. Carta, G.; Ubiera, A.; Pabst, T. Protein mass transfer kinetics in ion exchange media: Measurements and interpretations. *Chemical Engineering and Technology* 28, 1252-1264 (2005).
28. Bowes, B.D.; Lenhoff, A.M. Protein adsorption and transport in dextran-modified ion-exchange media 1. Adsorption. Submitted, *J. Chrom A*.
29. Forrer, N. et al. Investigation of the Porosity Variation during Chromatographic Experiments. *Industrial & Engineering Chemistry Research* 47, 9133-9140 (2008).
30. Yao, Y.; Lenhoff, A.M. Pore size distributions of ion exchangers and relation to protein binding capacity. *Journal of Chromatography A*. 1126, 107-119 (2006).
31. Yuan, Y., Oberholzer, M.R., Lenhoff, A.M. Size does matter: Electrostatically determined surface coverage trends in protein and colloid adsorption. *Colloids and Surfaces A-Physicochemical and Engineering Aspects* 165, 125-141 (2000).
32. Xu, X.; Lenhoff, A.M. A predictive approach to correlating protein adsorption isotherms on ion-exchange media. *The Journal of Physical Chemistry B* 112, 1028-1040 (2008).
33. Xu, X. Protein adsorption isotherms and their effects on transport in cation-exchange chromatography, Ph.D. thesis, University of Delaware, Newark (2008).
34. Langford, J. et al. Chromatography of proteins on charge-variant ion exchangers and implications for optimizing protein uptake rates. *Journal of Chromatography A* 1163, 190-202 (2007).

35. Chang, C.; Lenhoff, A.M. Comparison of protein adsorption isotherms and uptake rates in preparative cation-exchange materials. *Journal of Chromatography A*. 827, 281-293(1998).
36. Tosoh Biosciences LLC Toyopearl GigaCap S-650M: Product Overview. (2008).
37. Tosoh Biosciences LLC Ion Exchange Chromatography: Toyopearl Resins for IEC. (2008).
38. Guiochon, G. The limits of the separation power of unidimensional column liquid chromatography. *Journal of Chromatography A* 1126, 6-49 (2006).
39. Armenante, P.M.; Kirwan, D.J. Mass transfer to microparticles in agitated systems. *Chemical Engineering Science* 44, 2781-2796(1989).
40. Sano, Y.; Usui, H. Interrelations among mixing time, power number, and discharge flow rate number in baffled mixing vessels. *Journal of Chemical Engineering of Japan* 18, 47-52 (1985).
41. Bruch, T. et al. Influence of surface modification on protein retention in ion-exchange chromatography: Evaluation using different retention models. *Journal of Chromatography A* 1216, 919-926(2009).
42. Yang, H.; Bitzer, M.; Etzel, M.R. Analysis of Protein Purification Using Ion-Exchange Membranes. *Industrial & Engineering Chemistry Research* 38, 4044-4050 (1999).
43. Lavalle, P. et al. Extended random sequential adsorption model of irreversible deposition processes: From simulations to experiments. *Proceedings of the National Academy of Sciences of the United States of America* 96, 11100-11105 (1999).
44. Hunter, A.; Carta, G. Protein adsorption on novel acrylamido-based polymeric ion-exchangers - IV. Effects of protein size on adsorption capacity and rate. *Journal of Chromatography A* 971, 105-116(2002).